



# Investigation of visible light photocatalytic degradation of organic dyes by MoS<sub>2</sub> nanosheets synthesized by different routes

ANJALI RANI<sup>1</sup>, KULVINDER SINGH<sup>2</sup> and PRIANKA SHARMA<sup>1,\*</sup>

<sup>1</sup>Department of Physics, School of Basic and Applied Sciences, Maharaja Agrasen University, Solan 174103, India

<sup>2</sup>Department of Chemistry, School of Basic and Applied Sciences, Maharaja Agrasen University, Solan 174103, India

\*Author for correspondence (royprianka04@gmail.com)

MS received 23 October 2020; accepted 11 January 2021

**Abstract.** In this work, we have synthesized MoS<sub>2</sub> nanosheets (NSs) through hydrothermal as well as liquid-phase sonication methods and studied their ability to degrade organic dyes, methyl red (MR) and methylene blue (MB) under visible light irradiation. The as-synthesized photocatalysts have been characterized by powder X-ray diffraction, Raman Spectroscopy and transmission electron microscopy to confirm their structure and surface morphology. XRD patterns show that crystalline nature of MoS<sub>2</sub> NSs prepared by hydrothermal method appears at 160°C for 15 h. In contrast, sharp and intense diffraction peaks appear for liquid exfoliation method even at room temperature, exhibiting better crystallinity of the as-prepared NSs. The difference ( $\Delta$ ) of  $\sim 25\text{ cm}^{-1}$  between E<sub>2g</sub><sup>1</sup> and A<sub>1g</sub> modes of Raman spectra indicates formation of 5–6 layers of MoS<sub>2</sub> from both the synthesis routes. UV–Vis spectroscopy has been utilized to study the degradation of dyes by MoS<sub>2</sub> NSs as catalyst. Hydrothermally assisted synthesis of MoS<sub>2</sub> NSs exhibit lesser degradation efficiency with 58.92% for MR and 49.28% for MB, while exfoliation-assisted MoS<sub>2</sub> NSs act as better photocatalyst with 63.40 and 62.40% degradation of MR and MB, respectively. Faster degradation rate for MR compared to MB has been attributed to the presence of lesser chromophoric sites in MR.

**Keywords.** Photocatalysis; hydrothermal method; liquid exfoliation-photodegradation; percentage degradation; rate constant.

## 1. Introduction

Photocatalysis proves to be an efficient technique for the degradation of variety of pollutants present in effluent water released from industries [1,2]. Semiconductor nano catalysts, such as CdS, TiO<sub>2</sub>, SnO<sub>2</sub>, etc. have been widely used as photocatalyst due to their wide band gap, high sensitivity and antibacterial activity [3–7]. However, restricted responsivity towards excitation by UV light and fast rate of electron–hole recombination limit their use [8,9]. Thus, an alternative candidate is always searched for, which will overcome the limitations of semiconductor photocatalysts and show improved degradation efficacy.

In this context, transition metal dichalcogenides (TMDC), particularly MoS<sub>2</sub>, proves to be a promising candidate for photocatalysis of dyes [10,11]. Its tuneable band gap compresses the electron–hole recombination rates, thereby giving MoS<sub>2</sub> a unique property of getting self-excited under visible and UV light irradiation [5,12]. Compact degree of MoS<sub>2</sub> structure increases the surface area for charge carrier mobility, leading to strong adsorption of dye molecules on the MoS<sub>2</sub> catalyst surface [13]. Since the catalyst's surface structure greatly influences the charge transfer processes responsible for the

catalytic activity and affects the photocatalysis kinetics and its mechanism, hence, preparation of MoS<sub>2</sub> with specific morphology has attracted lot of interest [14,15]. Till now, various routes for synthesizing MoS<sub>2</sub> have been reported, such as mechanical exfoliation, liquid exfoliation, hydrothermal, chemical vapour deposition (CVD) and sulphurization method, etc. [16–18]. However, hydrothermal synthesis proves to be quite an effective technique for synthesizing nanostructures of 2D TMDC. Ntakadzeni *et al* [19] have fabricated PEGylated MoS<sub>2</sub> nanosheets (NSs) hydrothermally for photodegradation of organic dyes. Recently, Luo *et al* [20] have studied the hydrothermal synthesis of MoS<sub>2</sub> with controllable morphologies and its adsorption properties for bisphenol A. Ho *et al* [21] have fabricated MoS<sub>2</sub> nanoparticles using *in situ* photoreduction and deposition method to evaluate photocatalysis activity. The foremost advantage of the hydrothermal method is its ability to synthesize MoS<sub>2</sub> with different morphologies [20,22], having many reactive edge states exposed for enhanced chemical activities in different environments for practical applications [23–25]. Therefore, this synthetic route is more favoured due to its advantage of forming functional nanocomposites of TMDC with other semiconducting materials like

TiO<sub>2</sub>, carbon nanotubes (CNTs), graphene, etc. [26–28]. Hydrothermal method shows flexibility of controlling the morphological features, which depend upon various parameters like precursor, additives, temperature, reaction time, solvents, substrates, etc., on the growth mechanism of 2H-MoS<sub>2</sub> [14]. However, besides all the advantages of the hydrothermal synthesis route, its major disadvantage is forming an uncontrolled number of layers and non-uniform morphology with poor crystallinity that affects the fabrication of quickly modulated optical devices for practical applications [29]. Hence, an alternative synthesis route needs to be considered for improving the crystallinity of MoS<sub>2</sub> NSs at low reaction temperature, while maintaining uniformity over number of layers of these 2D materials, thereby, making it suitable for high-performance applications. Liquid-phase exfoliation overcomes the disadvantages of the hydrothermal synthesis route. It proves to be an efficient synthesis route for controlling the number of layers and maintaining uniformity avoiding aggregation of layers [17]. Sonication-assisted exfoliation with suitable solvent or in aqueous solutions, followed by centrifugation, helps in getting few layered MoS<sub>2</sub> NSs at room temperature with better crystallinity [30,31]. Since, the solvent chosen in sonication-assisted exfoliation helps to stabilize the exfoliated NSs against re-aggregation, providing more reactive edge sites for longer time, thus MoS<sub>2</sub> NSs exfoliated by this synthesis approach can be predicted to show enhanced photocatalytic response. Various researchers have reported hydrothermal synthesis routes to prepare MoS<sub>2</sub> nanostructures for photocatalytic applications [19–21, 28,32–35]. But, not much work has been done to investigate the photocatalytic activity of MoS<sub>2</sub> NSs exfoliated by liquid-phase sonication method.

In this study, we have attempted to exploit both the hydrothermal and the liquid-sonication method for exploring the effect of synthesis routes on the photocatalytic application of MoS<sub>2</sub> NSs for the degradation of organic dyes methyl red (MR) and methylene blue (MB). The results will help us to choose an appropriate synthesis route for large-scale industrial application of MoS<sub>2</sub> NSs to treat organic pollutants present in wastewater by photocatalysis.

## 2. Experimental

**Materials:** Analytical grade chemical reagents were used without further purification. Ammonium molybdate tetrahydrate [(NH<sub>4</sub>)<sub>6</sub>Mo<sub>7</sub>O<sub>24</sub>·4H<sub>2</sub>O], thiourea [CH<sub>4</sub>N<sub>2</sub>S], molybdenum disulphide (MoS<sub>2</sub>) powder (2 μm), ethanol, N-methyl 2-pyrrolidone (NMP) and isopropyl alcohol (IPA) were purchased from Sigma Aldrich. MR and MB were obtained from Molychem, India. Solutions were prepared in deionized water.

### 2.1 Synthesis of MoS<sub>2</sub> NSs by hydrothermal method

MoS<sub>2</sub> NSs were synthesized via conventional hydrothermal route using starting precursors: ammonium molybdate tetrahydrate as the source of molybdenum and thiourea as the source of sulphide ions. Briefly, 0.1 M solution of ammonium molybdate tetrahydrate and 0.5 M solution of thiourea were separately prepared in 40 ml of deionized water followed by mixing and sonication for 30 min. The sonicated solution was then transferred into a 100 ml Teflon-lined stainless-steel autoclave and the reaction was carried out in a muffle furnace for 15 h at 120, 140 and 160°C. The reaction was also carried out at 160°C for 7, 11 and 15h. After natural cooling of the furnace, the resulting dark brown precipitates were obtained through filtration. The precipitates were further washed with deionized water and absolute ethanol to remove any traces of residual ions. The final product was then dried at 60°C for 7 h.

### 2.2 Exfoliation of MoS<sub>2</sub> NSs by liquid-exfoliation method

MoS<sub>2</sub> NSs have been exfoliated via liquid-phase exfoliation method. In this process, 0.05 g of bulk MoS<sub>2</sub> powder was dispersed in 20 ml of NMP and ethanol:distilled water (volume ratio 1:1) in two different sets. The solution was ultrasonicated at room temperature with samples collected at 6, 12, 18, 24 and 30 h. The resultant dispersion was centrifuged at 3000 rpm for about 10 min to remove the residual large size MoS<sub>2</sub> powders. Further, the remaining solution was centrifuged at 10,000 rpm for 5 min. The supernatant was collected for further characterization to separate the black products. After 24 h of sonication, the colour changes from dark greyish black to greenish.

### 2.3 Photocatalytic test for dye degradation

Organic dyes MR and MB are poorly biodegradable and chemically stable contaminants present in effluent wastewater. We have used these organic dyes (MR and MB) model reactions to investigate the photocatalytic performance of MoS<sub>2</sub> NSs. The dye concentration of 50 ml of MR and MB in 100 ppm aqueous solution was treated with 0.01 g of MoS<sub>2</sub> NSs dispersed in 1 ml of distilled water for the MoS<sub>2</sub> NSs obtained from hydrothermal synthesis route. However, for liquid-sonication method, 1 ml of exfoliated MoS<sub>2</sub> NSs in NMP and ethanol:water was treated with the above concentration of dyes. Both the dye-catalyst solutions have been treated in dark as well as under white light (85-watt compact fluorescent lamp) for different exposure times (30, 60, 90 and 120 min). After treatment, the solutions were centrifuged for 10 min at 4000 rpm to remove the residual photocatalysts. Thus, obtained dye solutions were used to investigate the photocatalytic performance of the MoS<sub>2</sub> NSs prepared by hydrothermal and liquid exfoliation

methods for different exposure time using absorption spectroscopy.

#### 2.4 Characterization techniques

X-ray diffractometer (XRD) with  $\text{CuK}\alpha$  radiation ( $\lambda = 0.154$  nm) was used to determine the crystalline structure of as-prepared samples in the  $2\theta$  range from 10 to  $70^\circ$ . Transmission electron microscope (TEM) JEOL 2100F operated at 200 kV was used to analyse the morphologies of  $\text{MoS}_2$ . A confocal Raman spectrometer having an excitation source of 532 nm laser was used to investigate the vibrational modes of  $\text{MoS}_2$ . The UV-Vis absorption spectrophotometer (Labtronics, LT-2700, India) was used to record the absorption spectra of  $\text{MoS}_2$  and even for the photocatalytic study.

### 3. Results and discussion

#### 3.1 Structural investigations of $\text{MoS}_2$ NSs prepared by hydrothermal method

The  $\text{MoS}_2$  NSs were synthesized at different temperatures with variation in hydrothermal reaction time. The XRD patterns of hydrothermally synthesized  $\text{MoS}_2$  are presented in figure 1. In figure 1a, b and c, XRD patterns of  $\text{MoS}_2$  NSs are observed for samples prepared at temperatures 120, 140 and  $160^\circ\text{C}$  with hydrothermal reaction time maintained for 15 h. It is observed that at low hydrothermal temperatures of 120 and  $140^\circ\text{C}$ , diffraction peaks appear at 14.85 and  $28.21$  ( $2\theta$  degrees), corresponding to (002) and (004) crystal planes with many extra peaks. Though this exhibits the formation of  $\text{MoS}_2$  NSs, concentration of synthesized  $\text{MoS}_2$  is quite low at low reaction temperature. However, with increase in hydrothermal temperature to  $160^\circ\text{C}$ , all diffraction peaks of  $\text{MoS}_2$  are distinctly observed at 14.85, 28.13, 32.89, 33.78, 36.19, 39.82, 44.33, 49.97, 56.19, 58.44, 60.70, 62.96 ( $2\theta$  degrees) which arise from (002), (004), (100), (101), (102), (103), (006), (105), (106), (110), (008) and (107) crystal planes and matches well with JCPDS no. 37-1492 [8]. Higher intensity of (002) diffraction peak, as temperature increases from 120 to  $160^\circ\text{C}$ , attributes to the presence of random stacking of single layers of  $\text{MoS}_2$ . No other extra diffraction peaks are observed for  $\text{MoS}_2$  NSs at  $160^\circ\text{C}$ -15 h that reveals presence of no impurities in the sample at this temperature. XRD patterns are also observed for  $\text{MoS}_2$  NSs with variation in hydrothermal reaction time from 7 to 15 h maintained at  $160^\circ\text{C}$  in figure 1d, e and f. Here also, proper diffraction peaks do not appear exhibiting exact structure of  $\text{MoS}_2$  NSs for lower reaction time of 7 and 11 h, but as the hydrothermal reaction time increases to 15 h maintained at  $160^\circ\text{C}$ , peaks of  $\text{MoS}_2$  NSs appear. Hence, it can be concluded that the minimum condition required for synthesis of

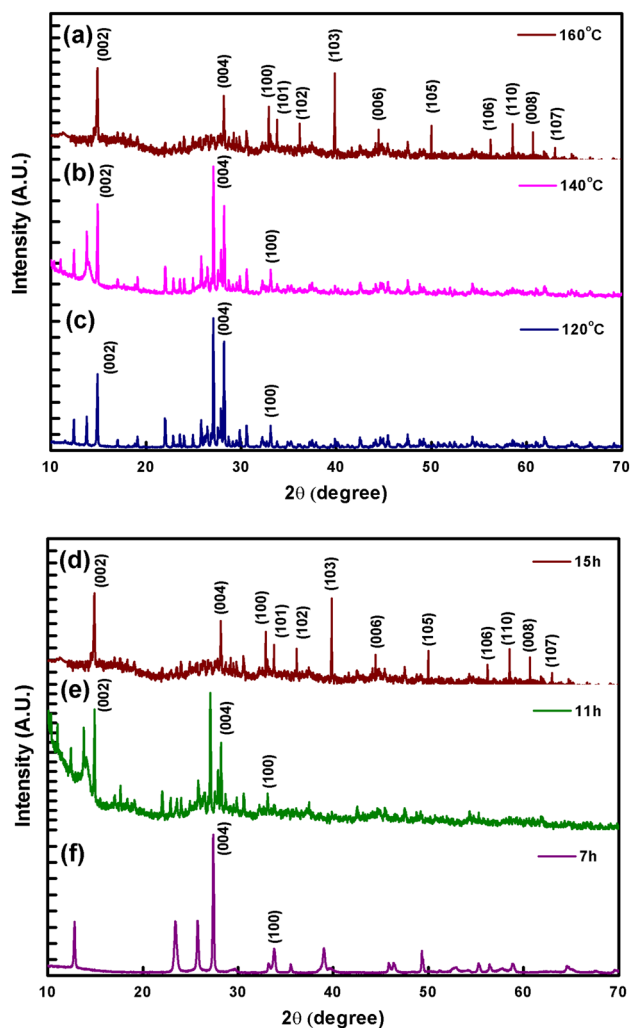


**Figure 1.** XRD patterns of  $\text{MoS}_2$  NSs (a, b and c) at different hydrothermal temperatures and (d, e and f) for different hydrothermal reaction times.

pure 2H- $\text{MoS}_2$  NSs with better crystallinity is  $160^\circ\text{C}$ -15 h. TEM results also provides direct evidence about the structural attributes of the sample. Figure 2a exhibits the TEM image of  $\text{MoS}_2$  NSs prepared hydrothermally at  $160^\circ\text{C}$  for 11 h. It is observed that  $\text{MoS}_2$  NSs are not properly formed within 11 h of hydrothermal reaction time at  $160^\circ\text{C}$ . In contrast, figure 2b exhibits the appearance of curled nanosheets of  $\text{MoS}_2$  indicating crystallization of  $\text{MoS}_2$  NSs at  $160^\circ\text{C}$ -15 h accompanied without any impurities. TEM results are in good agreement with the XRD results.

#### 3.2 Optical investigations of $\text{MoS}_2$ NSs prepared by hydrothermal method

Raman spectroscopy is an important technique for illustrating the vibrational modes and the number of layers of  $\text{MoS}_2$  NSs. In figure 3a, two typical Raman peaks for  $E_{2g}^1$  and  $A_{1g}$  modes appear at  $381.04$  and  $406.09$   $\text{cm}^{-1}$  with

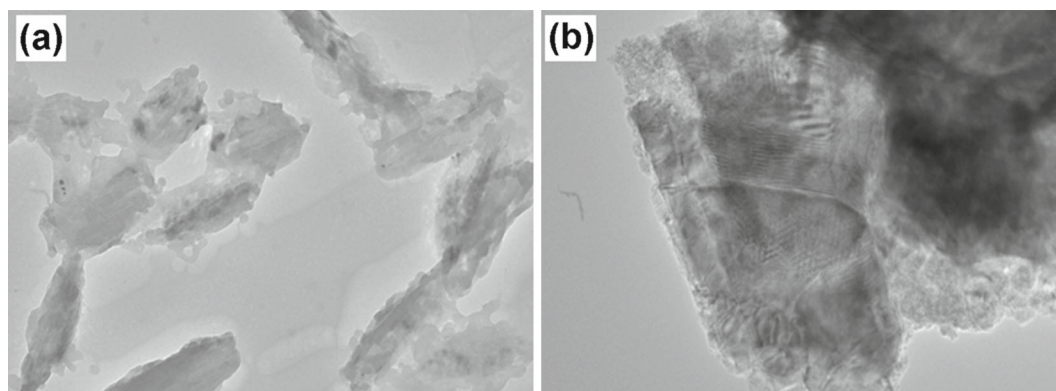


**Figure 2.** TEM image of the MoS<sub>2</sub> NSs prepared hydrothermally at 160°C for (a) 11 h and (b) 15 h.

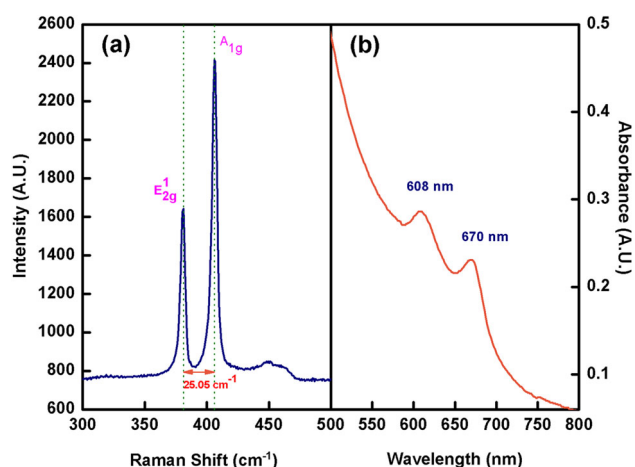


**Figure 3.** (a) Raman spectra and (b) absorption spectroscopy of the MoS<sub>2</sub> NSs prepared hydrothermally at 160°C for 15 h.

sharp intensity indicating material's crystallinity 160°C-15 h. The difference ( $\Delta$ ) of  $\sim 25 \text{ cm}^{-1}$  appears between the  $E_{2g}^1$  and  $A_{1g}$  modes, indicating the presence of 5–6 layers of MoS<sub>2</sub> [35].

UV–Vis spectroscopy was used to analyse the absorption spectra of MoS<sub>2</sub> NSs. Figure 3b shows the occurrence of two peaks of MoS<sub>2</sub> around 608 and 670 nm due to spin-orbit splitting corresponding to the excitonic transitions related to band gap of the material [35]. This indicates the absorbance ability of MoS<sub>2</sub> NSs in both UV and visible spectrum range that can be further exploited to use these MoS<sub>2</sub> NSs as photocatalysts for the pollutant's degradation.

### 3.3 Structural investigations of MoS<sub>2</sub> NSs exfoliated by liquid-phase sonication method

A few layered MoS<sub>2</sub> NSs were exfoliated from bulk in two different solvents NMP and ethanol:water sonicated for 24 h. The XRD patterns of these exfoliated MoS<sub>2</sub> NSs are presented in figure 4a and b. From figure 4a, diffraction peaks of exfoliated MoS<sub>2</sub> in NMP are observed at 29.80, 32.71, 33.54, 35.91, 39.59, 44.17, 49.82, 56.01, 58.37,

60.44, 62.81 for  $2\theta$  (degree). However, from figure 4b diffraction peaks of exfoliated MoS<sub>2</sub> are slightly displaced to 29.20, 32.89, 33.68, 36.08, 39.75, 44.33, 49.98, 56.17, 58.50, 60.61, 62.96 for ethanol:water as solvent. These diffraction peaks for both the solvents arising from crystal planes of (004), (100), (101), (102), (103), (006), (105), (106), (110), (008) and (107) and matches well with the JCPDS no. 37-1492, respectively [32]. These sharp and intense diffraction peaks present in both the solvents infer to better crystalline nature of the exfoliated MoS<sub>2</sub> NSs from the sonication method than the hydrothermal method. The shape and size of MoS<sub>2</sub> NSs were investigated using TEM. Figure 5a and b displays the TEM images of exfoliated MoS<sub>2</sub> NSs in ethanol:water and NMP, respectively. Figure 5a and b reveals the successful formation of sheet-like structure of MoS<sub>2</sub> NSs in ethanol:water and NMP, respectively. Figure 5b shows that the lattice spacing of MoS<sub>2</sub> NSs exfoliated in NMP comes out to be of the order of 0.27 nm corresponding to (100) plane.

### 3.4 Optical investigations of MoS<sub>2</sub> NSs exfoliated by liquid-phase sonication method

Figure 4c shows the Raman spectra of exfoliated MoS<sub>2</sub> NSs in two different solvents, NMP and ethanol:water. For ethanol:water, the in-planer  $E_{2g}^1$  mode appears at  $382.27 \text{ cm}^{-1}$ , while the out-planer  $A_{1g}$  mode appears at  $407.54 \text{ cm}^{-1}$ . In solvent NMP, the  $E_{2g}^1$  mode of the exfoliated NSs of MoS<sub>2</sub> slightly blue shifts to  $382.91 \text{ cm}^{-1}$ . However, the  $A_{1g}$  mode appears at the same position at  $407.54 \text{ cm}^{-1}$ . The Raman modes show high sensitivity towards thickness of layer. Generally, with decrease in number of layers, the difference between the  $E_{2g}^1$  and  $A_{1g}$  peaks decreases [35]. The Raman shift appears to be  $25.27 \text{ cm}^{-1}$  for MoS<sub>2</sub> NSs exfoliated in ethanol:water. This shift slightly decreases to  $24.63 \text{ cm}^{-1}$  in case of exfoliated MoS<sub>2</sub> NSs in NMP, which indicates decrease in the number of exfoliated layers for NMP as compared to ethanol:water system. However, from difference between the two modes, it can be inferred from previously reported works that bulk MoS<sub>2</sub> is exfoliated to

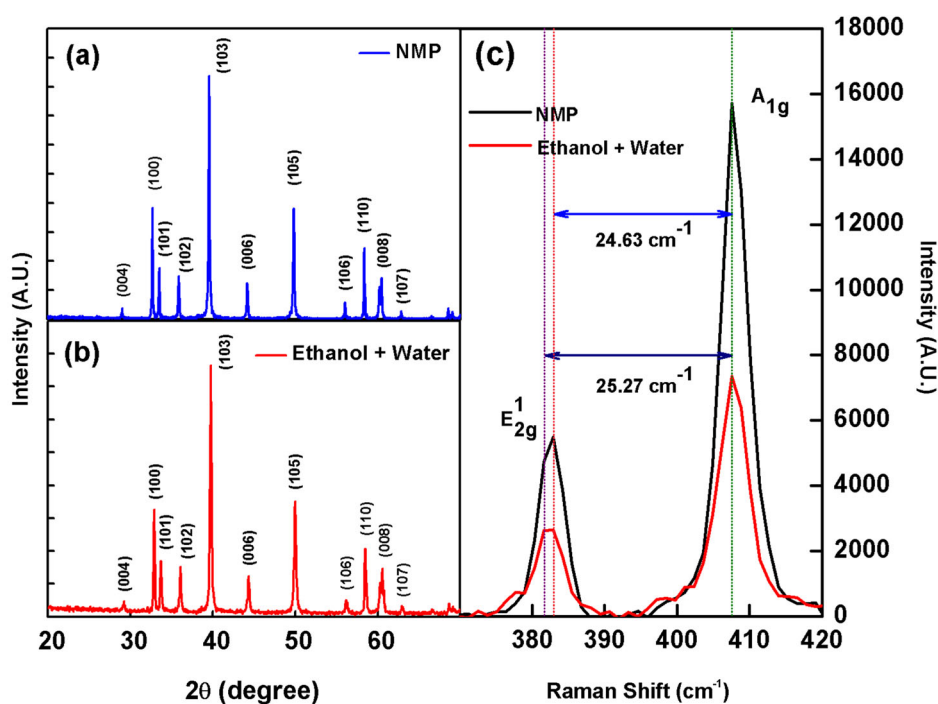


**Figure 4.** (a and b) XRD patterns of exfoliated MoS<sub>2</sub> NSs in NMP and ethanol: water and (c) Raman spectra of exfoliated MoS<sub>2</sub> NSs in NMP and ethanol:water.

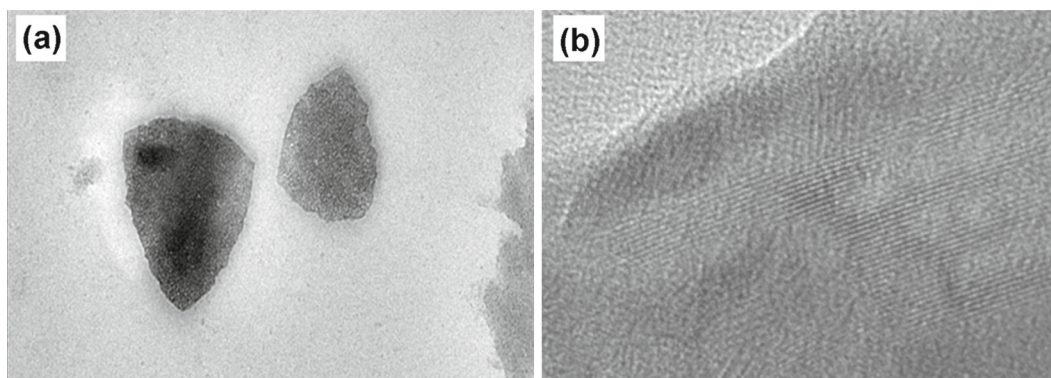


**Figure 5.** TEM images of MoS<sub>2</sub> NSs exfoliated in (a) ethanol:water and (b) NMP.

few-layer NSs with number of layers  $<5$  in both the solvents [30]. The  $E_{2g}^1/A_{1g}$  peak intensity ratio for MoS<sub>2</sub> NSs is 0.94 for both the solvents; therefore, by using Tuinstra Koenig relation, crystallite size measured is 17.82 nm. Sonication time is a key parameter for achieving high exfoliation ratio. To verify the exfoliation effect caused by sonication time, we have tailored the time of sonication from 6 to 30 h with same concentration of MoS<sub>2</sub>. The prepared samples were analysed for their optical properties by UV–Vis spectra in 400–800 nm. Figure 6a and b shows the absorption spectra of exfoliated MoS<sub>2</sub> NSs with increasing sonication time from 6 to 30 h in ethanol:water and NMP, respectively. All the spectra exhibit three absorption bands. One of the broad band centred around 460 nm in both the solvents is attributed to direct electronic

transition between conduction and valence band energy level. Two typical MoS<sub>2</sub> peaks appear around 624–626 and 685 nm, for ethanol:water. However, in NMP as solvent, slight blue shift is exhibited in these peaks, which appears around 606–616 and 670–683 nm. Appearance of these peaks indicates the formation of MoS<sub>2</sub> NSs and is attributed to the transitions that occur due to spin-orbit splitting [34]. By increasing the sonication time to 24 h, the optical absorbance increases, but at 30 h, some decrease in absorbance spectra is observed. Therefore, it can be concluded that increasing the time of sonication leads to an increase in NSs scission, reducing both the lateral dimension and thickness of the exfoliated sheets to an extent. However, further increase of sonication time leads to decrease in absorbance. Hence, analysing the absorbance spectra, we

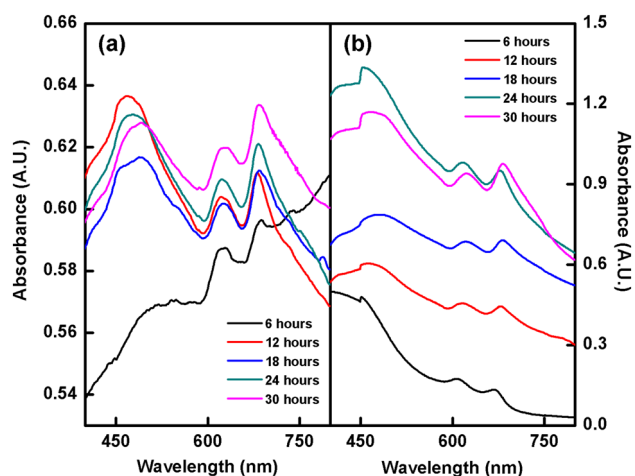


**Figure 6.** UV-Visible spectra of the MoS<sub>2</sub> NSs exfoliated in (a) ethanol:water and (b) NMP.

have decided to use exfoliated MoS<sub>2</sub> NSs obtained at 24 h of sonication for measuring the degradation efficiency of organic dyes MR and MB.

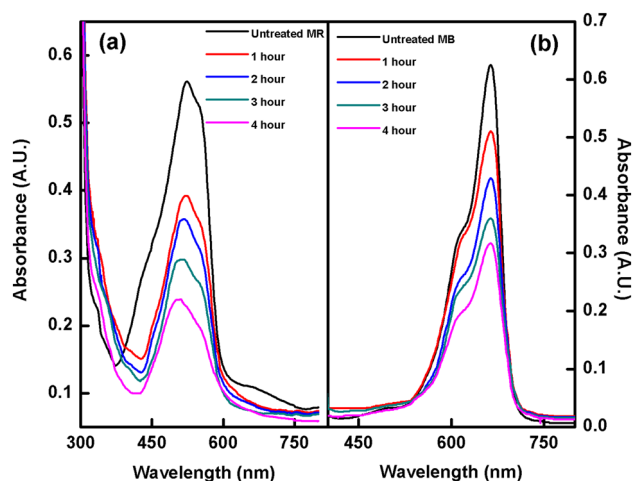
### 3.5 Photocatalytic activity of MoS<sub>2</sub> NSs under visible light irradiation

The photocatalytic activity of MoS<sub>2</sub> NSs prepared by two different synthesis routes, hydrothermal and exfoliation in ethanol:water and NMP were investigated under visible light irradiation (85-watt compact fluorescent lamp) for organic dyes MR and MB using UV-Vis spectrophotometer. The intensity of the characteristic absorption peak of MR at 522 and 665 nm for MB is used to track their degradation efficiency, respectively. A blank test has been undertaken in the absence of catalyst showing negligible self-degradation of the dyes. No noticeable change in colour

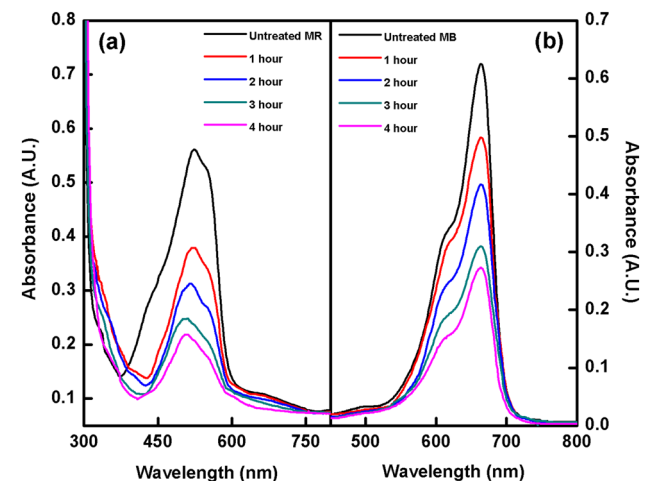
is observed between untreated and treated dye solutions of MR and MB when placed in dark as compared to visible light irradiation for 4 h. Figure 7a and b shows the absorption spectra of MoS<sub>2</sub> NSs prepared hydrothermally as catalyst for the degradation of MR and MB carried out for 4 h. By adding hydrothermally prepared MoS<sub>2</sub> NSs, the absorption edge shifts towards lower wavelength (495 nm) for MR and correspondingly, intensity of the absorption peak decreases rapidly as the irradiation time increases, as shown in figure 7a. However, in case of MB as shown in figure 7b, the absorption edge shows no noticeable change. In contrast, decrease in intensity of the absorption peak is observed gradually with an increase in irradiation time up to 4 h.

Figure 8a and b displays absorption spectra of degradation of MR and MB dye by MoS<sub>2</sub> NSs exfoliated in ethanol:water, respectively. Similarly, figure 9a and b exhibits a decline in MR and MB dye absorption spectra, indicating respective degradation of dyes by exfoliated MoS<sub>2</sub> NSs in NMP. Irradiating with white light, intensity of the absorbance peak for MR shows a declining trend along with blue shifting of the absorption edge towards lower wavelength of 504 nm for MoS<sub>2</sub> NSs exfoliated in ethanol:water as shown in figure 8a. Similarly, from figure 9a, MoS<sub>2</sub> NSs exfoliated in NMP, the absorption edge blue shifts to 502 nm, exhibiting a decrease in the absorption peak. In case of MB (figures 8b and 9b), there is no noticeable change in edge of the absorption peak of dye solution treated with MoS<sub>2</sub> NSs exfoliated in ethanol:water as well as in NMP under white light irradiation. However, similar decrease in absorption peak is observed with an increase in irradiation time (4 h) for MB.

The degradation efficiency of dyes MR and MB treated with MoS<sub>2</sub> NSs prepared hydrothermally and exfoliated in solvents ethanol:water and NMP are measured using Beer-Lambert's law. According to this law, absorbance is proportional to concentration of dye. Hence, percentage



**Figure 7.** Absorption spectra of the degradation of (a) MR dye and (b) MB dyes; for 4 h by MoS<sub>2</sub> NSs prepared hydrothermally.



**Figure 8.** Absorption spectra of the degradation of (a) MR and (b) MB dyes by MoS<sub>2</sub> NSs exfoliated in ethanol:water.

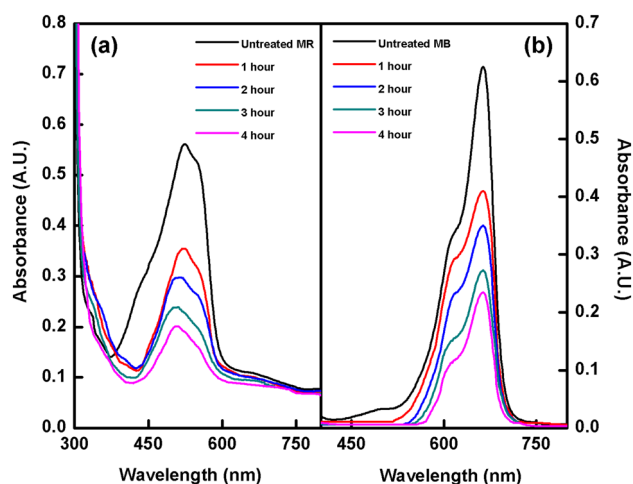


**Figure 9.** Absorption spectra of the degradation of (a) MR and (b) MB dyes by MoS<sub>2</sub> NSs exfoliated in NMP.

degradation efficiency can be calculated by using equation (1) [33].

$$R = \frac{C_0 - C}{C_0} \times 100\% = \frac{A_0 - A}{A_0} \times 100\%, \quad (1)$$

where  $C_0$ ,  $C$ ,  $A_0$ ,  $A$  are concentration and absorbance of dye at initial time 0 and after  $t$  minutes, respectively.

Figure 10a exhibits percentage degradation of organic dyes MR and MB by hydrothermally synthesized MoS<sub>2</sub> NSs irradiated under white light (85-watt CFL) for 4 h. Correspondingly, degradation of both the dyes is clearly visible in the pictorial representation presented in figure 10b. Initially, degradation of dye MB is quite low 18.40% for 1 h, but with increase in irradiation time, degradation of MB increases from 18.40 to 49.28%. Similarly, degradation of MR increases from 30.35 to 58.92% in 4 h. This reveals that though MR degrades better than MB by hydrothermally synthesized MoS<sub>2</sub> NSs as a catalyst, but efficiency is quite low and longer time may be needed for complete degradation of both the dyes.

For investigating better degradation of dyes, exfoliated MoS<sub>2</sub> NSs by liquid-exfoliation method has been utilized. The percentage degradation of MR and MB by MoS<sub>2</sub> NSs exfoliated in ethanol:water and NMP under white light irradiation are shown in figure 11a and b. Degradation of both the dyes in 4 h is quite visible from continuous fading of dye colour represented in the pictorial description in figure 12a and b, respectively. It is observed that MR degrades from 32 upto 61.04% in 4 h, whereas degradation of MB enhances upto 56.30% for same time duration, starting initially from 20.30% in 1 h for ethanol:water. A similar degradation trend has been observed for MoS<sub>2</sub> NSs exfoliated in NMP for both the dyes MR and MB. In NMP, degradation of MR increases from 36 to 63.40%, and MB degrades from 34.40 to 62.40% in 4 h of irradiation. It has been explored that though degradation efficiency of dyes increases with exfoliated MoS<sub>2</sub> NSs, however, the

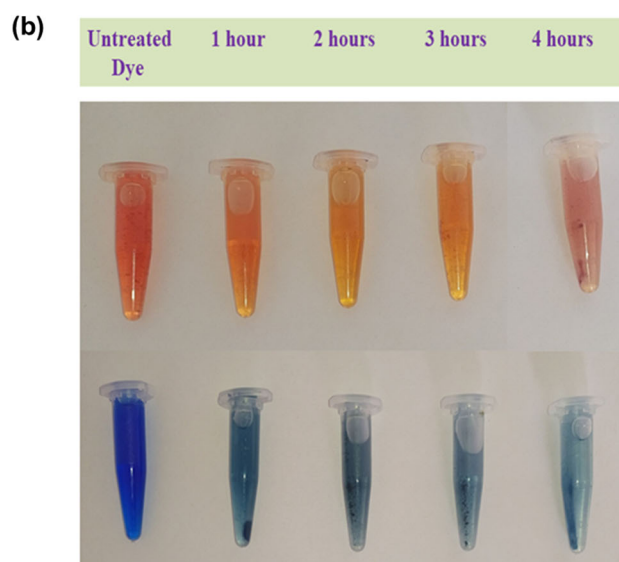
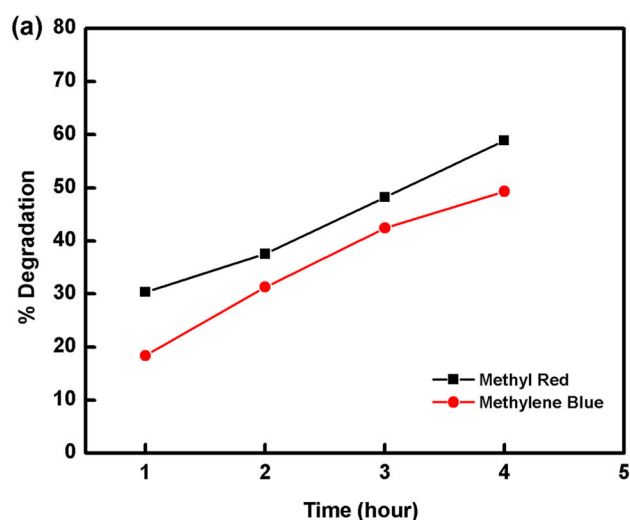


**Figure 10.** (a) Percentage degradation of MR and MB dyes by MoS<sub>2</sub> NSs synthesized by hydrothermal method and (b) their pictorial representation.

degradation efficiency of MR still shows better degradation trend than MB, similar to hydrothermally synthesized MoS<sub>2</sub> NSs.

Comparative degradation efficiency of hydrothermally synthesized and exfoliated MoS<sub>2</sub> NSs in both the solvents ethanol:water and NMP are presented in tables 1 and 2. From both the tables, it is clear that solvent-assisted liquid exfoliation of MoS<sub>2</sub> NSs proves to be better photocatalyst than hydrothermally synthesized MoS<sub>2</sub> NSs. From XRD data of the hydrothermal synthesis route, it has been observed that MoS<sub>2</sub> NSs with better crystallinity are prepared at minimum 160°C for 15 h and higher temperature. At this temperature, there might be expansion of the inter-layer distance of MoS<sub>2</sub> NSs, indicating expansion of lattice. Due to high surface energy and attracting Van der Waals interaction, there will be aggregation of MoS<sub>2</sub> layers during

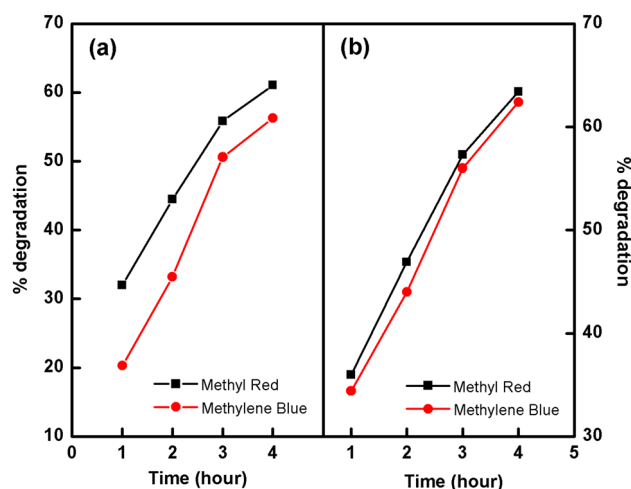


**Figure 11.** Percentage degradation of MR and MB dyes by MoS<sub>2</sub> NSs exfoliated in (a) ethanol + water and (b) NMP.

fabrication. As a result, hydrothermally synthesized MoS<sub>2</sub> NSs might lose many of its active sites essentially needed for the photocatalytic activity. Whereas, the surface area of the NSs exfoliated by sonication method is quite increased and the solvent used to sonicate NSs prevent aggregation of sheets, thereby providing more active sites for reaction with dye molecules. Thus, availability of more active sites due to lesser non-aggregation of sheets in liquid exfoliation sonication method might be the reason for improved photocatalytic activity of this method compared to hydrothermally synthesized MoS<sub>2</sub> NSs. However, in liquid exfoliation sonication, MoS<sub>2</sub> NSs exfoliated in NMP exhibits better degradation efficiency than the MoS<sub>2</sub> NSs exfoliated in ethanol:water system. Coulombic repulsion is created due to charged sites between neighbouring sheets, disrupting the bonding between the interlayer basal planes. Therefore,

**Table 1.** Comparative percentage degradation of MR under visible light irradiation.

Time (h)	Percentage degradation of MR under visible light irradiation		
	Hydrothermal	Ethanol:water	NMP
1	30.35	32.00	36.00
2	37.50	44.50	46.90
3	48.21	55.80	57.30
4	58.92	61.04	63.40

**Table 2.** Comparative percentage degradation of MB under visible light irradiation.

Time (h)	Percentage degradation of MB under visible light irradiation		
	Hydrothermal	Ethanol:water	NMP
1	18.40	20.30	34.40
2	31.30	33.20	44.00
3	42.40	50.60	56.00
4	49.28	56.30	62.40

high-dipole solvents like NMP offers better electrostatic stabilization of NSs. Also, the O<sub>2</sub> molecule present in NMP leads to an increase in moisture content of the solution, which improves the quality of the exfoliated layers by sonication in NMP. Thus, the exfoliated layers are smoother and more even than those obtained by ethanol:water promoting formation of redox-active species *in situ*. At the same time, there is an auto-oxidation pathway that converts NMP into N-methyl succinimide with intermediate

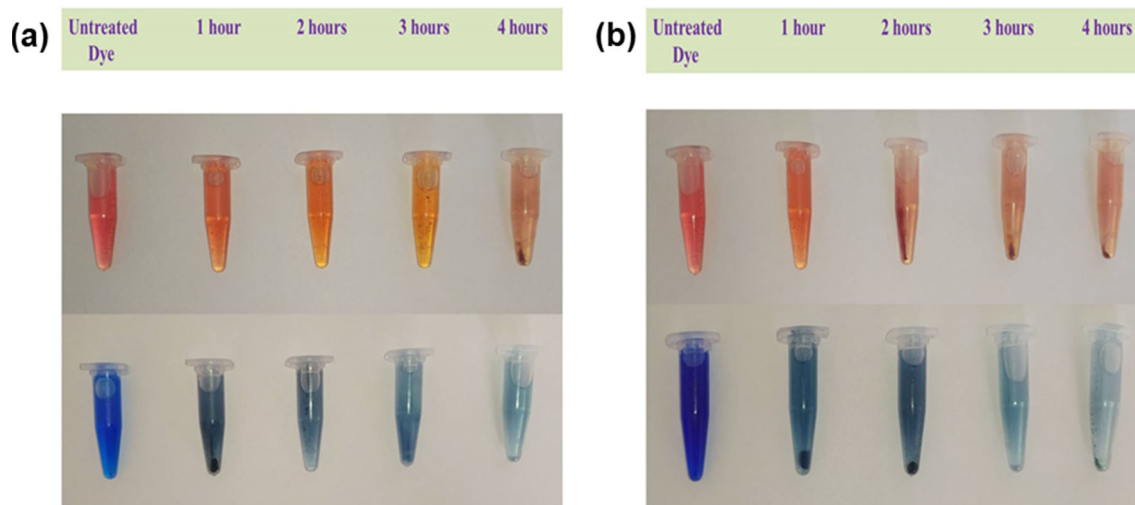


**Figure 12.** Pictorial representation of the degradation of MR and MB dyes by MoS<sub>2</sub> NSs exfoliated in (a) ethanol + water and (b) NMP.



hydroperoxide, leading to appearance of highly reactive sites that aids the exfoliation process as the edge sites due to oxidation.

The degradation efficiency can be better understood from the kinetic studies of MR and MB adsorption by MoS<sub>2</sub> NSs obtained from both the methods. The constant rate *k* of the degradation was calculated using equation (2),

$$\ln \frac{C}{C_0} = -kT. \tag{2}$$

C<sub>0</sub> is the initial concentration and *C* the concentration at time *t*, *k* the rate constant and *T* the irradiation time. A graph is plotted between normalized absorption *C/C*<sub>0</sub> and time of irradiation given by equation (2) that explains the type of order of reaction followed by the degradation of dyes with photocatalysts.

Figure 13a and b exhibits the kinetic graph of MR and MB with photocatalysts MoS<sub>2</sub> NSs obtained by hydrothermal and sonication methods. The figures reveal that normalized absorption declines exponentially with time, which exhibits that degradation reaction obeys pseudo-first-order reaction [8]. The degradation behaviour of both the dyes

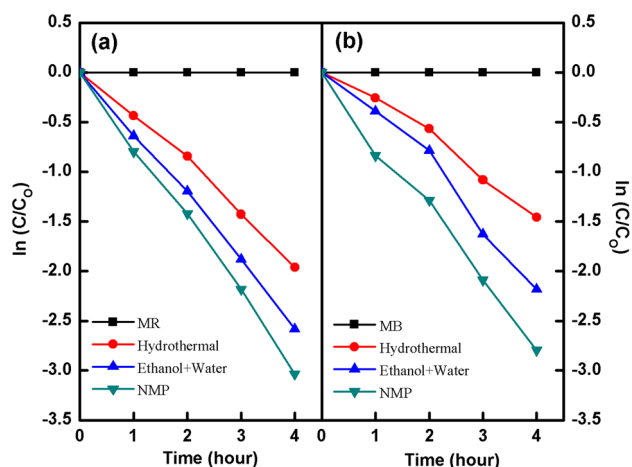


**Figure 13.** Kinetic graph of (a) MR dye and (b) MB dyes with MoS<sub>2</sub> NSs obtained by hydrothermal and sonication methods as photocatalysts.

**Table 3.** Comparative kinetic rate constant values for degradation of MR and MB with MoS<sub>2</sub> NSs obtained by hydrothermal and sonication methods as photocatalysts.

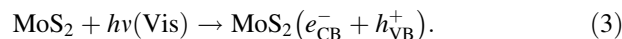
Synthesis routes	Rate constant values for degradation of dyes (h <sup>-1</sup> )	
	MR	MB
Hydrothermal	0.9333	0.6723
Liquid exfoliation (ethanol:water)	1.2595	0.9974
Liquid exfoliation (NMP)	1.4881	1.4022

follows the same trend. Values of rate constant calculated from kinetic graphs are compiled in table 3. The rate constant values show that time taken for degradation of MR is 0.9333 h<sup>-1</sup> faster than MB, which is 0.6723 h<sup>-1</sup> for hydrothermally prepared MoS<sub>2</sub> photocatalyst. Similarly, the reaction rate of MoS<sub>2</sub> (ethanol:water) photocatalyst for MR degradation is 1.2595 h<sup>-1</sup>, while for MB, it is 0.9974 h<sup>-1</sup>. In the same way, MoS<sub>2</sub> (NMP) has rate of reaction of 1.4881 h<sup>-1</sup>, however, for MB, it is 1.4022 h<sup>-1</sup>. Hence, these rate constant values confirm that the reaction rate is faster for MR than MB.

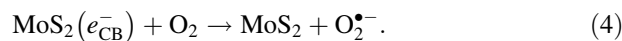
Degradation of dyes depend upon the presence of chromophoric sites. MR has only one chromophoric site, while there are four chromophoric sites present in MB. During the photocatalysis process, the 'OH or O<sub>2</sub><sup>-</sup> radicals generated, attack these chromophoric sites present in dyes to destabilize or break the dyes into reducible components. Hence, lesser number of chromophoric sites present in MR leads to faster destabilization of the dye for photocatalytic degradation under white light irradiation.

#### 4. Photocatalytic degradation mechanism

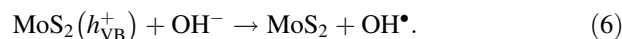
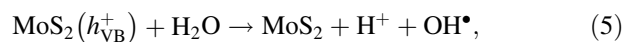
Photocatalytic degradation behaviour of organic dyes under irradiation by visible light may proceed via two possible processes: photocatalytic oxidation and photosensitized oxidation. In the former mechanism, when MoS<sub>2</sub> NSs are irradiated by visible light, the photoexcitation of the semiconductor leads to the generation of electron-hole pair (*e*<sub>CB</sub><sup>-</sup> from the conduction band and *h*<sub>VB</sub><sup>+</sup> from the valence band) on the surface of the catalyst given by equation (3):



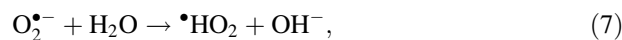
Oxygen vacancies on catalyst surface act as a trap for electrons to inhibit electron-hole recombination. The photo-generated electrons oxidize with O<sub>2</sub> (sink for electron acceptors) adsorbed on the MoS<sub>2</sub> surface leading to the formation of superoxide radical anion (O<sub>2</sub><sup>•-</sup>) given by equation (4):



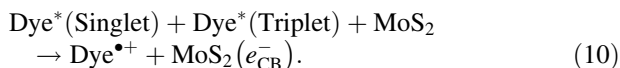
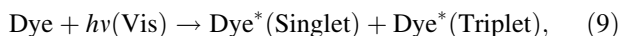
The photoinduced hole can be easily oxidized by the organic molecule or react with H<sub>2</sub>O or OH<sup>-</sup> ion to oxidize to hydroxyl radical (OH<sup>•</sup>) given by equations (5) and (6).



Finally, the hydroxyl radical (OH<sup>•</sup>) and the superoxide radical anions (O<sub>2</sub><sup>•-</sup>) are responsible for the overall photodecomposition reaction given by equations (7) and (8).



On the other hand, in the photosensitizing mechanism, instead of catalyst, the adsorbed dye itself gets excited to singlet or triplet states under visible light irradiation. It injects electrons to the conduction band of MoS<sub>2</sub> nanostructures given by equations (9 and 10).



The cationic dye radical (Dye<sup>•+</sup>) undergoes degradation to hydroxyl radical (OH<sup>•</sup>). The hydroxyl radical (OH<sup>•</sup>) from both the mechanisms actively break the various bonds present in organic dyes and leads to mineralization. Both the mechanisms of photo-oxidation and photosensitization go side by side. It is not possible to explain which of the mechanism is superior. Still, it is established that the photosensitizing mechanism improves the efficiency of photo-oxidation degradation of dyes and makes the process more feasible.

## 5. Conclusion

In summary, MoS<sub>2</sub> NSs have been synthesized by two routes: hydrothermal and liquid-phase sonication. Degradation of organic dyes MR and MB by MoS<sub>2</sub> NSs synthesized by both the routes have been studied by illumination under UV–Vis light. The as-synthesized photocatalysts characterized by XRD reveal that the exfoliated NSs from the sonication method at room temperature exhibit sharp and intense diffraction peaks inferring better crystallinity than NSs prepared at 160°C–15 h by conventional hydrothermal method. For both the synthesis routes, the difference ( $\Delta$ ) of  $\sim 25 \text{ cm}^{-1}$  appears between the E<sub>2g</sub><sup>1</sup> and A<sub>1g</sub> modes of Raman spectra, indicating the presence of 5–6 layers of MoS<sub>2</sub>. Among these three routes, hydrothermally synthesized MoS<sub>2</sub> NSs exhibit least degradation efficiency with 58.92% for MR and 49.28% for MB. Simultaneously, the exfoliated MoS<sub>2</sub> NSs in NMP act as a better photocatalyst for the degradation with 63.40% for MR and 62.40% for MB. Lesser efficiency of the MoS<sub>2</sub> NSs prepared by the hydrothermal method might be due to re-aggregation of sheets and availability of lesser number of active sites essentially needed for the photocatalytic activity.

On the other hand, in high-dipole solvent NMP, the O<sub>2</sub> molecule present in NMP promotes the formation of redox-active species leading to appearance of highly reactive edge sites enhancing the photocatalytic degradation of both the dyes. It is also observed that MR shows faster degradation ability with rate constant 0.9333 and 1.4881 h<sup>-1</sup> than MB with rate constant 0.6723 and 1.4022 h<sup>-1</sup> for hydrothermal method and liquid sonication with NMP, respectively. Better degradation of MR might be

attributed to the presence of lesser chromophoric sites than MB.

## References

- [1] Sharma M, Mohapatra P K and Bahadur D 2017 *Front. Mater. Sci.* **11** 366
- [2] Zhu S and Wang D 2017 *Adv. Energy Mater.* **7** 1700841
- [3] Xu C, Ravi Anusuyadevi P, Aymonier C, Luque R and Marre S 2019 *Chem. Soc. Rev.* **48** 3868
- [4] Altintas Yildirim O, Arslan H and Sönmezoğlu S 2016 *Appl. Surf. Sci.* **390** 111
- [5] Vattikuti S V P and Byon C 2016 *Superlattices Microstruct.* **100** 514
- [6] Tab A, Bellal B, Belabed C, Dahmane M and Trari M 2020 *Optik (Stuttg).* **214** 164858
- [7] Malligavathy M, Iyyapushpam S, Nishanthi S T and Padiyan D P 2018 *Pramana–J. Phys.* **90** 1
- [8] Rani A, Singh K, Patel A S, Chakraborti A, Kumar S, Ghosh K *et al* 2020 *Chem. Phys. Lett.* **738** 136874
- [9] Sumesh C K and Parekh K 2019 *Pramana–J. Phys.* **92** 87
- [10] Mishra A K, Lakshmi K V and Huang L 2015 *Sci. Rep.* **5** 15718
- [11] Quinn M D J, Ho N H and Notley S M 2013 *ACS Appl. Mater. Interfaces* **5** 12751
- [12] Johari P and Shenoy V B 2012 *ACS Nano* **6** 5449
- [13] Li Z, Meng X and Zhang Z 2018 *J. Photochem. Photobiol. C: Photochem. Rev.* **35** 39
- [14] Li M, Wang D, Li J, Pan Z, Ma H, Jiang Y *et al* 2016 *RSC Adv.* **6** 71534
- [15] Paul K K, Sreekanth N, Biroju R K, Narayanan T N and Giri P K 2018 *Sol. Energy Mater. Sol. Cells* **185** 364
- [16] Chhowalla M, Shin H S, Eda G, Li L-J, Loh K P and Zhang H 2013 *Nat. Chem.* **5** 263
- [17] Prabukumar C, Mohamed Jaffer Sadiq M, Krishna Bhat D and Udaya Bhat K 2019 *Res. Express* **6** 085526
- [18] Ding Q, Czech K J, Zhao Y, Zhai J, Hamers R J, Wright J C *et al* 2017 *ACS Appl. Mater. Interfaces* **9** 12734
- [19] Ntakadzeni M, Anku W W, Kumar N, Govender P P and Reddy L 2019 *Bull. Chem. React. Eng. Catal.* **14** 142
- [20] Luo L, Shi M, Zhao S, Tan W, Lin X, Wang H *et al* 2019 *J. Saudi Chem. Soc.* **23** 762
- [21] Ho W, Yu J C, Lin J, Yu J and Li P 2004 *Langmuir* **20** 5865
- [22] Hou S X, Wu C and Huo Y J 2017 *Ceram. - Silikaty* **61** 158
- [23] Huang Q, Liu X, Chen Z, Gong S and Huang H 2019 *Chem. Phys. Lett.* **730** 608
- [24] Chaudhary N, Khanuja M, Abid and Islam S S 2018 *Sens. Actuator. A: Phys.* **277** 190
- [25] Luo S, Dong S, Lu C, Yu C, Ou Y, Luo L *et al* 2018 *J. Colloid Interface Sci.* **513** 389
- [26] Sabarinathan M, Harish S, Archana J, Navaneethan M, Ikeda H and Hayakawa Y 2017 *RSC Adv.* **7** 24754
- [27] Chen M, Dai Y, Wang J, Wang Q, Wang Y, Cheng X *et al* 2017 *J. Alloys Compd.* **696** 900
- [28] Kaur M, Umar A, Mehta S K and Kansal S K 2019 *Appl. Catal. B: Environ.* **245** 143
- [29] Peng Y, Meng Z, Zhong C, Lu J, Yu W, Jia Y B *et al* 2001 *Chem. Lett.* **30** 772

- [30] Nguyen T P, Sohn W, Oh J H, Jang H W and Kim S Y 2016 *J. Phys. Chem. C* **120** 10078
- [31] Mukherjee S, Maiti R, Midya A, Das S and Ray S K 2015 *ACS Photonics* **2** 760
- [32] Tian Y, He Y and Zhu Y 2004 *Mater. Chem. Phys.* **87** 87
- [33] Singh R, Barman P B and Sharma D 2017 *J. Mater. Sci. Mater. Electron.* **28** 5705
- [34] Eda G, Yamaguchi H, Voiry D, Fujita T, Chen M and Chhowalla M 2011 *Nano Lett.* **11** 5111
- [35] Lee C, Yan H, Brus L E, Heinz T F, Hone J and Ryu S 2010 *ACS Nano* **4** 2695